NANO LETTERS

Letter

pubs.acs.org/NanoLett

Nanostructured Stealth Surfaces for Visible and Near-Infrared Light

Z. Diao,[†] M. Kraus,[‡] R. Brunner,[‡] J.-H. Dirks,[†,§] and J. P. Spatz*[,†]

[†]Department of Cellular Biophysics, Max Planck Institute for Medical Research, Heidelberg, and Laboratory of Biophysical Chemistry, University of Heidelberg, Jahnstraße 29, 69120 Heidelberg, Germany

[‡]University of Applied Sciences Jena, Carl Zeiss Promenade 2, 07745 Jena, Germany

Supporting Information

ABSTRACT: So far, all previous attempts to apply nanostructures for perfect transmission have not achieved maximum transmittance beyond 99.5% due to the limited regularity of the nanoscale surface geometry: too low for many high-end applications. Here we demonstrate a nanostructured stealth surface, with minimal reflectance (<0.02%) and maximal transmittance (>99.8%) for a wavelength range, covering visible and near-infrared. Compared to multilayer thin film coatings for near-infrared applications our antireflective surfaces operate within a much broader wavelength range, are mechanical stable to resist human touch or contamination, show a 44% higher laser-induced damage threshold, and are suitable for bended interfaces such as microlenses as well.

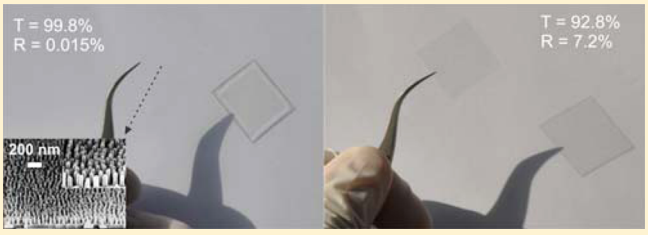

KEYWORDS: *Antireflection, block copolymer micelle lithography, near-infrared, laser-induced damage threshold, nanostructures, moth eye*

Moth-eye inspired subwavelength nanostructures are frequently used to reduce reflection and improve transmission or absorption of various optical interfaces.[1−6] In particular, there is a high demand for optical materials that offer perfect transmission and antireflection properties or, equivalently, minimum absorption in the visible to near-infrared wavelength range. Applications include high power laser, touch display, stealth, imaging, and spectroscopy systems.[7−10]

Conventional antireflection coatings usually consist of a thin film of dielectric material which is coated onto optical substrates. These layers reduce optical losses caused by a sudden change of the refractive index at the interface when light passes from one medium to another. Unfortunately, these multilayer coatings offer antireflection (AR) properties only in a relatively narrow wavelength range, and furthermore they are also limited to small variations of the incidence angle. As an alternative to the multilayer AR approaches, Lord Rayleigh discovered that layers with gradually changing effective refractive indices could also improve the antireflection properties of optical surfaces by aiming for refractive index matching between the two interfacing optical media. Ever since this discovery, different top-down and bottom-up methods with subwavelength spatial resolution have been used to fabricate antireflective coatings.[11−14] However, most work using this technology focused on improving either antireflection, transmission, or absorption, and all of these within a limited wavelength range. Current interface fabrication methods, providing nearly perfect transmission and at the same time ultralow reflection over a broad wavelength range including the near-infrared range, so far still do not reach the required optical quality. Combining high transmission, low reflectivity, and low absorption is a very desired optical quality for many high-energy and sensitive optical applications, such as high power laser systems, optical sensing systems, human touch displays, light extraction devices, and potential stealth applications.[15−17]

Block copolymer micelle lithography (BCML) is a powerful method for preparing periodically spaced metallic nanoparticles with sub-100 nm spacing on different substrates.[18−20] Highly ordered arrays of nanoparticles are fabricated using BCML and used as etching masks in a reactive ion etching (RIE) process to obtain well-defined arrays of nanopillars perpendicular to the interface.[21] These nanopillars gradually adjust the difference in the refractive indices of the substrate material and the surrounding medium (e.g., vacuum, air, or water). Until today, the combination of BCML and RIE remains the method of choice for producing surfaces for antireflection applications in the ultraviolet (UV) and visible range. Using this physical principle enables increased light transmittance, reduced reflectance, and low absorption to be obtained within a range of wavelengths covering several hundred nanometers. The wavelength of maximal transmittance and minimal reflectance depends on the effective refractive index and the optical thickness of the layer that is made up of the nanopillar array. One strategy to tune the effective refractive index of this interface layer within a limited wavelength range is to adjust the spatial spacing and the width of the nanopillars.[22] Nevertheless, only certain combinations of these two parameters result in smooth gradient refractive index profiles. Such profiles, in turn, lead to high transmittance and low reflectance. However,

Received: August 6, 2016
Revised: September 24, 2016

DOI: 10.1021/acs.nanolett.6b03308
Nano Lett. XXXX, XXX, XXX−XXX

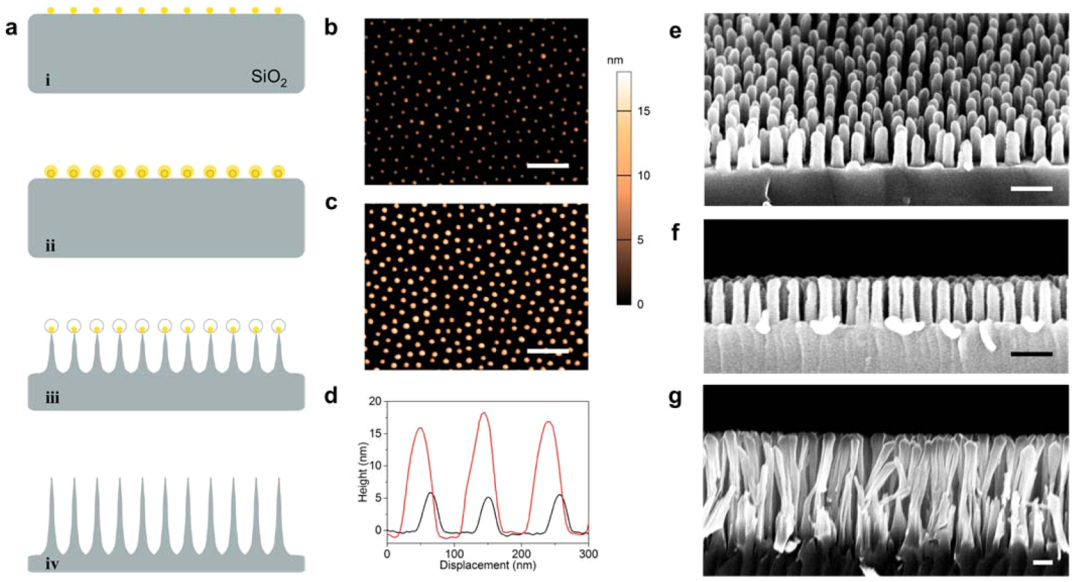

Figure 1. Nanopillar production. (a) Schematic illustration of nanopillar fabrication using BCML, electroless deposition, and RIE. (i) A quasi-hexagonal array of gold nanoparticles is prepared by BCML. (ii) The gold particles are grown larger by electroless deposition. (iii, iv) The gold particle pattern is used as an etching mask for RIE etching, resulting in nanopillars. (b) AFM image of a sample prepared by BCML (spacing 105 ± 12 nm, gold particle diameter 6.0 ± 0.2 nm). (c) AFM image of the same sample after 15 s of electroless growth (diameter 16.5 ± 0.8 nm). (d) Cross section measurement of the gold particles before (black line) and after 15 s of electroless growth (red line). (e, f, g) SEM images of two different nanopillar arrays: 25° tilted top view (top image) and side view (middle) of 350 nm sized nanopillars; side view of 1400 nm sized nanopillars (bottom). Scale bar: 200 nm.

optimization of the spatial spacing and the width of the nanopillars turns out to be an ineffective approach for improving the above-mentioned combination of optical properties. A second and very effective strategy to adjust the wavelength of the maximal transmittance and of the minimal reflectance is to alter the nanopillar height. So far, nanopillars prepared using a combination of BCML and RIE methods could only reach a maximum height of 500 nm due to the limited stability of the etching mask and/or the size of the metal particles.[21]

The method we describe here combines BCML with the electroless growth of gold nanoparticles.[23,24] The increase in gold particle size results in a thicker and more stable etching mask, thus allowing us to prepare much taller nanopillars with a height of up to 2 μm in fused silica. It is the first time such heights have been achieved in fused silica. Furthermore, our refined RIE etching process gives us excellent control over the geometry and refractive index profiles of our pillars. The quasi-hexagonal arranged Au nanoparticles are prepared by BCML on both sides of a fused silica substrate (see Figure 1). The particles are spaced 105 ± 12 nm apart. The diameter of the Au nanoparticles is increased from 6 ± 0.2 nm to 16.5 ± 0.8 nm in the following electroless growth process. Next, this quasi-hexagonal pattern of Au nanoparticles is transferred by RIE etching, thereby creating nanopillars on both sides of the substrate. In order to simultaneously control the height and profile of the nanopillars, etching protocols for different pillar heights were developed. Our refined technique results in nanopillars of fused silica with a defined height between 100 and 2000 nm.

In addition to the height, the geometrical profile of the nanopillars also strongly affects the interface's effective refractive index gradient.[4,25,26] Therefore, the defining (and most influential) parts of the nanopillar's shape are the bottom base and the top. When light passes vertically through an array of nanostructures, the geometrical profiles of the bottom and top parts determine how smooth the transitions between the refractive index of the substrate, the nanopillar layer, and the surrounding air are. In this study we compared three pillar types of identical height but with individual shapes (see Figure 2a). Each pillar consists of a Gaussian shaped bottom and top section, which can make up 5% (standard), 20% (rocket-ship), or 40% (bullhorn) of the total pillar height with gradient effective refractive index. The cylindrical middle section of the pillars is not associated with an effective gradient refractive index. Figure 2a compares the simulated optical transmittance of the three nanopillar types: the smaller the cylindrical middle part, the higher the resulting transmittance of the pillar structure. In Figure 2b the simulations are confirmed by experimental data. Nanopillars with the designed bullhorn profile display a smoother transition between the different parts of the pillar and a sharper tip as well as the highest transmittance. The quasi-cylindrical standard profile resulted in only 98.0%, the rocket-ship-like profile resulted in 99.5%, and our newly designed bullhorn profile achieved 99.8% transmittance. The standard profile acts like a single layer coating. It is well-known that a single layer with an effective refractive index can reach maximum transmission for a specific wavelength. For good comparability we used the same pattern parameter for all shown nanopillar shapes which are based on the real structures. This results in poorer transmittance than theoretically possible due to the nonideal effective refractive index for the given pillar height.

The height of the nanopillars defines the maximal transmittance and the minimal reflectance as a function of wavelength. By precisely controlling the pillar height to be between 100 and 2000 nm, the maximum transmittance can be adjusted over wavelengths ranging from 250 to 2500 nm (see Figure 2d). The experimental optical transmittance and reflectance of double-sided substrates with nanopillars of

DOI: 10.1021/acs.nanolett.6b03308
Nano Lett. XXXX, XXX, XXX−XXX

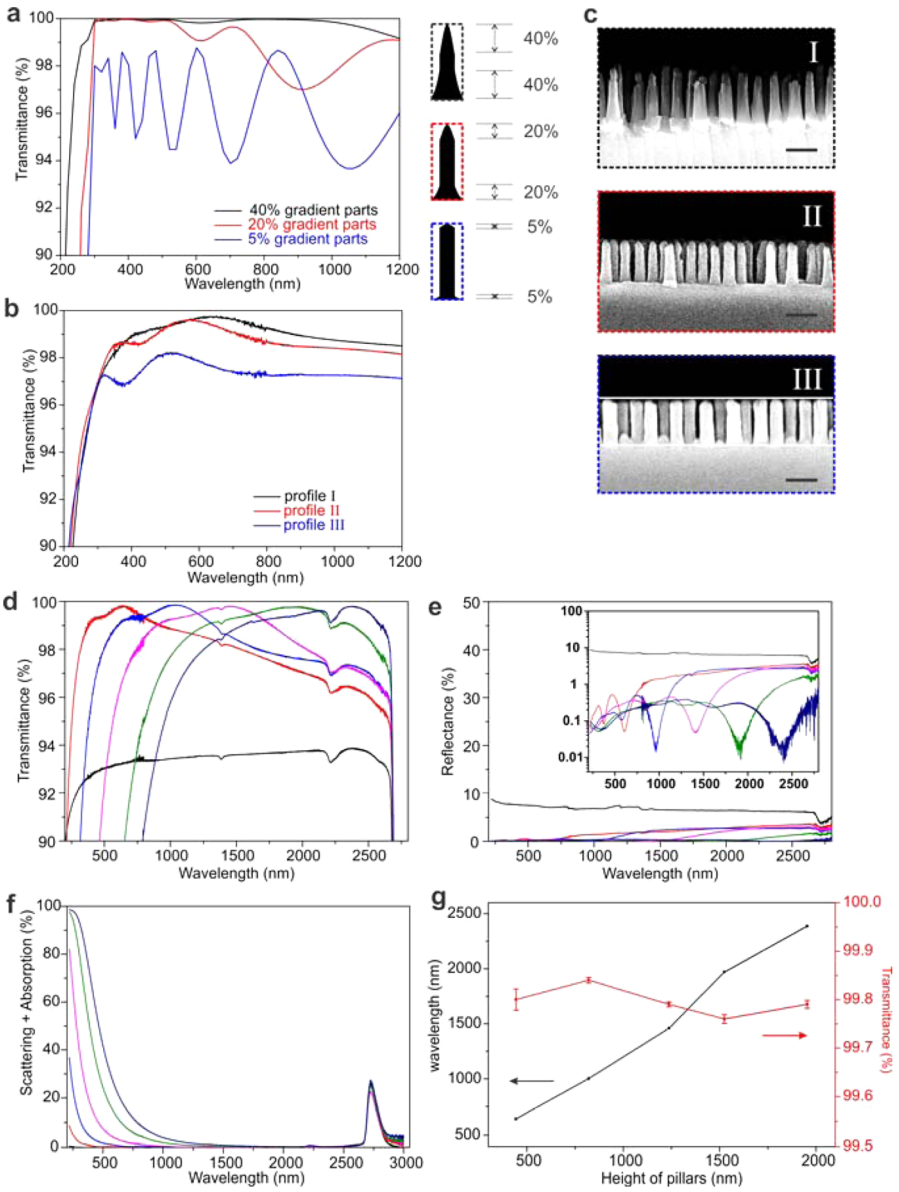

Figure 2. Nearly perfect transmittance and ultralow reflectance of substrates structured on two sides with nanopillars: effect of nanopillar shape and size. The drawing in the middle shows the profiles of the three differently shaped nanopillars and the height percentage of the top, middle, and the bottom base section of each pillar. (a) Simulated transmittance of a nanopillar substrate with bullhorn profile (black), a rocket-ship-like profile (red), and a quasi-cylindrical profile (blue). (b) Experimental measurements on a double-sided substrate with 450 nm nanopillars, confirming the results of the simulation shown in a. (c) SEM images of the three differently shaped nanopillar types. Scale bar: 200 nm. (d, e) Transmittance and reflectance (200−2800 nm) of a double-sided substrate with nanopillars of different heights: 450 nm (red), 780 nm (blue), 1250 nm (pink), 1520 nm (green), and 1950 nm (dark blue). The reference sample without nanopillars is shown in black. (f) Optical scattering and absorption of the same substrates as in d. and e. (g) Nanopillar height plotted against maximum transmittance (red triangles) and the wavelength in nanometers (black squares).

Table 1. Optical Maximal Transmittance (T_{max}) and Minimal Reflectance (R_{min}) of the Substrates Analyzed in Figures 2d and 2e

	450 nm[a]	780 nm[a]	1250 nm[a]	1520 nm[a]	1950 nm[a]
T_{max}	99.80%	99.84%	99.79%	99.76%	99.79%
ΔT_{max}	0.022%	0.006%	0.005%	0.009%	0.008%
wavelength T_{max}	644 nm	1036 nm	1448 nm	1955 nm	2386 nm
R_{min}	0.048%	0.016%	0.048%	0.019%	0.016%
ΔR_{min}	0.0016%	0.0033%	0.0012%	0.0055%	0.0067%
wavelength R_{min}	606 nm	963 nm	1411 nm	1907 nm	2418 nm

[a]Pillar height.

different heights are listed in Table 1. All of the tested substrates achieved a transmittance greater than 99.5% over a wavelength range spanning 250 nm. The breadth of this range increases with the height of the nanopillars. For 1950 nm sized nanopillars above 99.5% transmittance was achieved over a range of 450 nm. A nanopillar size of 150 nm led to high

DOI: 10.1021/acs.nanolett.6b03308
Nano Lett. XXXX, XXX, XXX−XXX

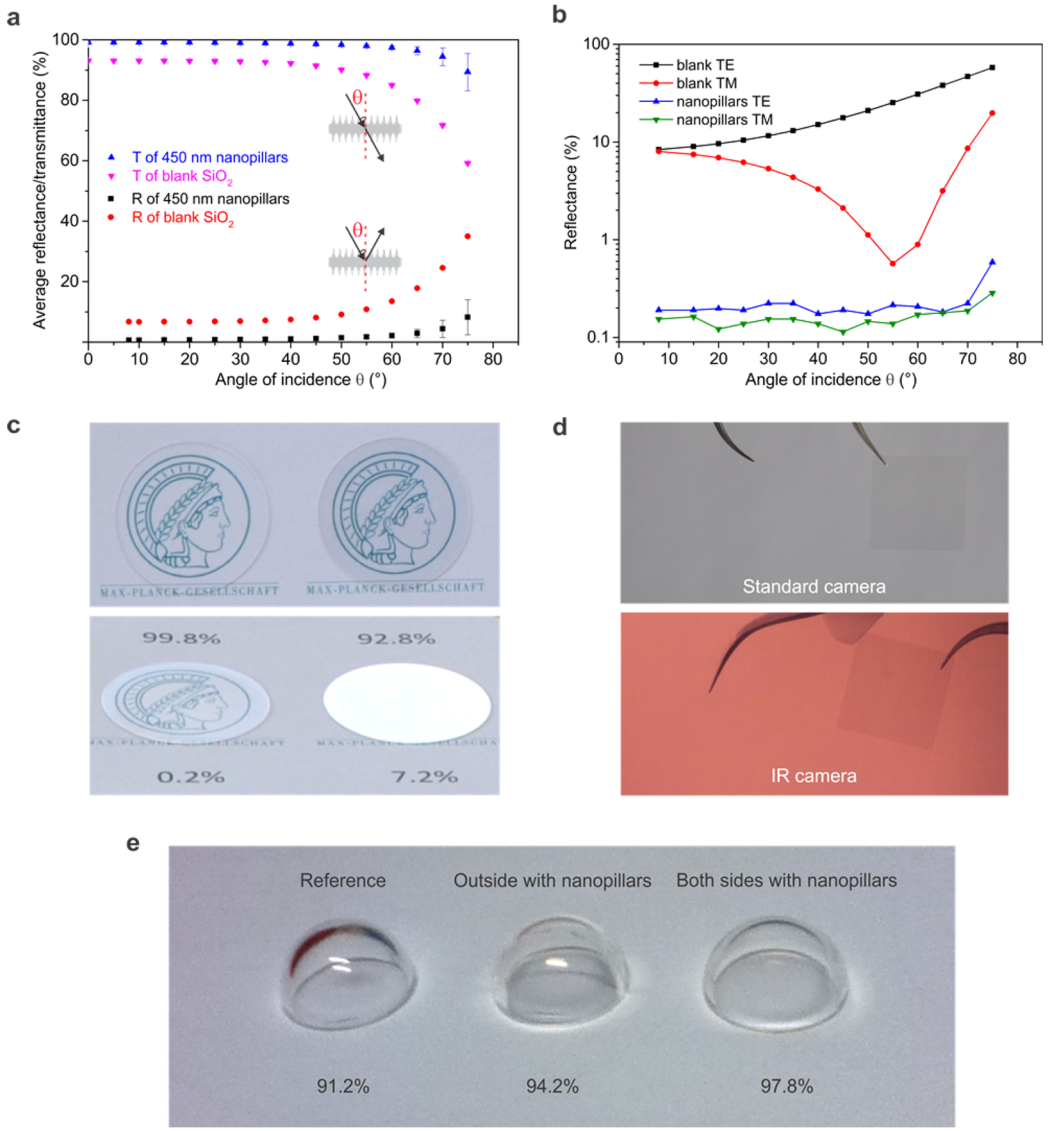

Figure 3. Transmittance and reflectance of substrates with nanopillars at various angles of incidence and different polarization states. (a) The average transmittance and reflectance of the substrate with 450 nm sized nanopillars (blue triangles and black squares) compared to a reference sample (pink triangles and red circles) measured at different wavelengths between 380 and 1000 nm and with different AOI between 0 and 75° (5° steps are depicted, reflectance starts at 8°). (b) The reflectance of the double-sided substrate with 1950 nm sized nanopillars compared to an unstructured reference sample measured at 680 nm wavelength and two different polarization states (TE and TM) with different AOI between 8 and 75° (5° steps are depicted). (c) Image of the Greek goddess Minerva as seen under a fused silica substrate with 450 nm nanopillars on both sides (left) compared to an unstructured reference (right). Each substrate has a diameter of 25 mm, matching the size of the drawing. The top set of images were taken at an observation angle of 0°, the bottom set of images at an observation angle of 30°. (d) 20 × 20 mm double-sided fused silica substrate with 780 nm nanopillars on both sides (left) compared to a 20 × 20 mm unstructured reference sample (right) as observed through a standard (top) and an IR camera (bottom). The nanostructured substrate is invisible with both the standard and the IR camera. (e) Image of the semispherical fused silica shell: unstructured (left), outside with 450 nm nanopillars, and both sides with 450 nm nanopillars. The maximal transmittance is 91.1%, 94.2%, and 97.8%, respectively. The diameter of the shell is 20 mm, thickness 1.0 mm.

transmittance in the UV range: 99.5% and 98.3% at 273 and 193 nm, respectively (see Figure S1). Nanopillar size also had an effect on the minimal reflectance of the substrate: 450 nm height resulted in a minimal reflectance of 0.048%, 780 nm height resulted in 0.016%, and 1950 nm in 0.016% minimal reflectance. The reflectance of the substrate equipped with 1950 nm sized nanopillars was <0.3% over a wavelength range from 200 to 2600 nm. Nevertheless, disorder concerning the pillar height and the uniformity of the spacing between pillars occurred relatively frequently during the production of higher pillars, resulting in higher scattering loss in short wavelength range (Figure 2f, deduced from Figures 2d and 2e). Between 1750 nm and shorter wavelengths the transmittance of long nanopillars decreased significantly. Even so, considering how broad the covered wavelength range is, the level of low reflectivity achieved with these nanostructures is remarkable. As shown in Figure 2g, an adjustable transmittance higher than 99.8% (99.9% for each air/fused silica interface) was achieved within a wavelength range from 500 to 2500 nm simply by altering the height of the nanopillars. The simultaneous optimization of transmittance, reflectance, wavelength, and pillar height has been achieved (see Figure S2). Compared to other antireflection techniques, which focus solely on achieving

DOI: 10.1021/acs.nanolett.6b03308
Nano Lett. XXXX, XXX, XXX−XXX

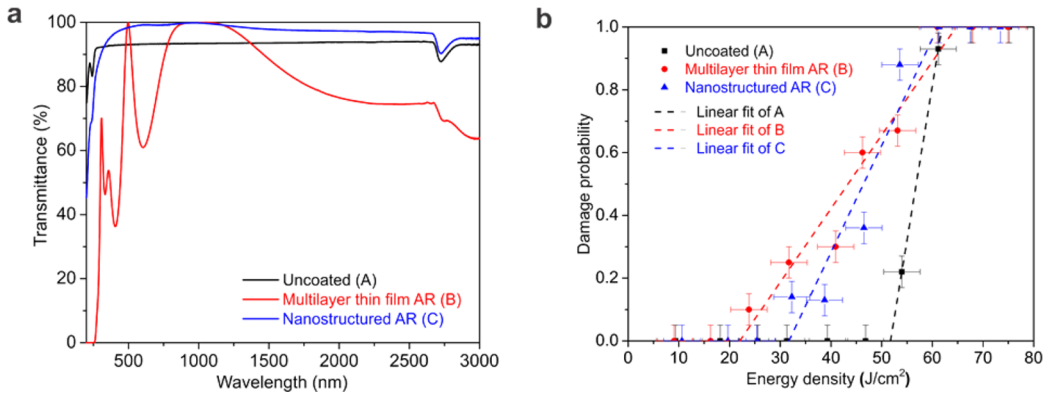

Figure 4. Laser-induced damage threshold measurements. (a) Transmittance (at wavelengths between 200−3000 nm) of an uncoated substrate (black), a sample with a multilayer thin film antireflection coating on both sides (red), and a substrate with 780 nm sized nanopillars on both sides (blue). (b) The laser damage probability of the same samples as in a. The laser was operated in pulse mode using different laser energy densities (laser wavelength 1064 nm, 5.5 ns, 50 Hz). The laser-induced damage thresholds were determined at 51.8 J/cm^2 (uncoated), 22.0 J/cm^2 (multilayer AR coating), and 31.8 J/cm^2 (nanostructured AR).

low reflectance, this is one of the key accomplishments of our method.

The optical performance of an antireflective surface at varied angle of incidence (AOI) and different polarization states is highly interesting for applications like solar cells, display screens, and different optical components.[27,28] We measured the average transmittance and reflectance of the double-side structured substrate bearing 450 nm sized nanopillars and compared it to that of an unstructured reference sample at different wavelengths between 380 and 1000 nm with different AOI between 0 and 75° (see Figure 3a). Especially at AOI angles >45° the fused silica with 450 nm nanopillars showed much better omnidirectional transmittance and antireflectance in comparison to blank substrates. Nanostructured surfaces are therefore better suited for applications that utilize higher light intensities and larger AOIs, e.g., for different sensor and solar applications. Another important characteristic of antireflective surfaces is how well they perform at different polarization states. The reflectance of TE (s-polarized) light and TM (p-polarized) light from a double-sided substrate with 1950 nm sized nanopillars is measured at 680 nm wavelength with an AOI that is incrementally increased in 5° steps starting at 8° up to 75°. The reflectance of the double-sided nanopillar substrate shows total polarization independence and nearly zero reflectance up to an AOI of 70° (see Figure 3b). A similar effect has been found on nanostructured silicone surfaces designed for better light absorption.[3]

The described effects can even be observed with the naked eye. Figure 3c shows an image of the Greek goddess Minerva as seen under a fused silica substrate with 450 nm nanopillars on both sides (left) compared to an unstructured reference (right). Each substrate has a diameter of 25 mm, matching the size of the drawing. The top set of images was taken at an observation angle of 0°, the bottom set of images at an observation angle of 30°. At 0° observation angle light is transmitted through both the nanostructured and the unstructured substrate, and in both cases the images below are visible. In the bottom set of images the unstructured reference substrate reflects the light to such an extent that the image of Minerva is not recognizable anymore. The substrate structured with nanopillars, in contrast, shows nearly perfect transmittance and almost-zero reflectance. Figure 3d shows a comparison of a fused silica substrate with 780 nm sized nanopillars (left) and an unstructured substrate (right) as observed through a standard and an IR camera. The nanopillar surface is practically invisible in the visible and near-infrared wavelength ranges (Figure 3d). Importantly, this method also can be used for highly curved surfaces. For an unstructured semispherical fused silica shell, two mirror images of the lamp reflected from both shell surfaces can be clearly observed. For a shell decorated with 450 nm nanopillars on one side or both sides, only one reflected mirror image or almost no reflected mirror image is observed on the shell (Figure 3e).

To assess the performance of antireflective nanostructures or coatings in applications with high energy lasers it is important to determine the laser-induced damage threshold (LIDT). The LIDT of a surface is defined as the point at which a laser is of sufficient intensity to start to produce a lasting change to the coated surface, which is observable at high magnification. LIDT depends on test wavelength, pulse width, repetition rate, and the inspection method and has always been a significant feature in laser design and laser operations.[29,30] Nanostructured surfaces for antireflection applications have two important advantages over multilayered thin film coatings in this respect. First, the nanostructures are etched into the substrate, hence, only one type of material and interface is involved so that absorbance is minimized. Second, the nanostructures increase the surface area of the substrate, resulting in a better heat transfer at the interface and thereby improving the LIDT. Figure 4 shows the probability of causing laser-induced damage on the fused silica substrates equipped with a multilayer thin film coating or nanostructures. Both are optimized for high transmission at a wavelength of 1064 nm and are evaluated using different laser energy densities. The LIDT of the samples with the multilayer thin film coating and the nanostructured substrate was 22 J/cm^2 and 31.8 J/cm^2, respectively. This shows that our nanostructured surface offers a much broader high-transmittance operation wavelength range and a 44% higher LIDT than a comparable substrate with the multilayer thin film coating. These two advantages are especially significant in new laser systems that operate with a broad range of wavelengths like white light laser beams[31] or when durability under a high operation power is required.[32] Finally, the mechanical stability of the nanopillar surfaces was qualitatively tested against human touch (see Figure S3). Hard pressing of a thumb against the nanostructured surface caused contamination which could be

DOI: 10.1021/acs.nanolett.6b03308
Nano Lett. XXXX, XXX, XXX−XXX

completely reversed by rinsing with ethanol. No lasting damage on the surface could be detected.

In conclusion, we have created fused silica substrates with nanopillars on both sides that achieve nearly perfect transmittance and ultrabroad near-zero reflectance by combining BCML, electroless deposition, and refined RIE etching methods. After further theoretical and experimental work, this method has the potential to be applied to other materials, such as optical glasses with a high refractive index, CaF_2, or even sapphire. With 99.8% transmittance and 0.02% reflectance at various incidence angles and states of polarization, this method is useful for numerous applications in optical systems, especially in the near-infrared range. Our measurements also show that nanopillar structured surfaces have an LIDT that is 44% higher than that of conventional multilayer coatings on the same fused silica substrate at 1064 nm wavelength. We believe that this finding is helpful for many laser applications, for example to increase efficiency and durability of high power laser systems.

Experimental Section. The software UNIGIT was used to conduct the theoretical investigations based on the method of rigorous coupled wave analysis (RCWA). The implemented solver supports 1- and 2-dimensional approaches. For the 2-dimensional simulation we created the nanopillar profile matrix in a unit cell of 128 × 128 data values and approximated the nanopillar height by 64 layers. The basic parameters of the simulated structures are lateral period 110 nm, diameter (full width half-maximum criterion) 70 nm, and absolute height 450 nm. The simulation was conducted with light illuminating under normal incidence with a wavelength varying between 200 and 3000 nm in steps of 20 nm. Using a convergence analysis for different comparable structures we found that 8 Rayleigh orders provide sufficient accuracy. Due to this we considered 8 Rayleigh orders for all the shown 2-dimensional calculations. The described simulations are suitable to model transmission and reflection effects at the nanostructured interface. The approach is not able to predict absorption or scattering losses due to disordered nanostructures.

Block copolymer micelle nanolithography (BCML) is used to prepare a hexagonal mask of gold nanoparticles by spin-coating. Polystyrene-*block*-poly (2/4)-vinylpyridine, PS-*b*-P2VP (M_n(PS) = 110000, M_n(PVP) = 70500, M_w/M_n = 1.09, Polymersource, Inc.) copolymers were dissolved in toluene with a concentration of 2 mg/mL at room temperature and stirred for 12 h to form spherical micelles. $HAuCl_4 \cdot 3H_2O$ (Sigma-Aldrich) was added to the solution with a loading rate of $L = 0.2$. After stirring for 24 h, the fused silica substrates (20 × 20 mm, thickness 0.17 mm) were spin-coated with the solution at 6000 rpm for 60 s.

On substrates used to produce nanopillars longer than 1000 nm, gold particles were grown for 30 s. When producing substrates with nanopillars shorter than 1000 nm, this growing step was omitted. For electroless deposition samples were first activated by hydrogen plasma treatment using a PVA TePla 1000 microwave plasma system (3 min, 0.4 mbar and 200 W). The activated samples were then immersed into a solution of 0.1% $HAuCl_4$/0.4 mM NH_3OHCl for 30 s. Prior to reactive ion etching, the copolymer shells were removed by hydrogen plasma treatment (45 min, 0.4 mbar and 350 W).

An Oxford Plasmalab 80 RIE etcher was used to transcribe the hexagonal patterns into nanopillars on the substrates. Two different etching steps were used to control the geometry and refractive index profile of the nanopillars. The first step consisted of two treatments, first with a 1:1 mixture of Ar and SF_6 (80 sccm, 50 mTorr, RF power 120 W, 60 s) followed by a 1:1 mixture of Ar and CHF_3 (80 sccm, 50 mTorr, RF power 120 W, ICP power 20 W, 20 s). The second step consisted of a single treatment with a 1:1 mixture of Ar and SF_6 (80 sccm, 50 mTorr, RF power 120 W, 80 s). Different cycles of these two steps were carefully combined until the desired structure depth was reached. The temperature of the sample was kept constant at 20 °C during the entire process.

A Cary5000 UV−vis−NIR spectrometer was used to measure the transmittance and reflectance (175−3300 nm). A specially designed OMT goniometer was used to determine the angle of incidence and the dependence on the polarization state (380−1100 nm, transmittance 0−90°, reflectance 8−85°).

■ ASSOCIATED CONTENT

Supporting Information

The Supporting Information is available free of charge on the ACS Publications website at DOI: 10.1021/acs.nanolett.6b03308.

Transmittance vs wavelength in the UV range, minimum reflectance vs nanopillar height and wavelength, cleaning of contamination caused by human touch, and importance of boosting transmittance (PDF)

■ AUTHOR INFORMATION

Corresponding Author

*E-mail: spatz@is.mpg.de.

Present Address

§J.-H.D.: Biomimetics-Innovation-Centre, Hochschule Bremen - City University of Applied Sciences, Neustadtswall 30, 28199 Bremen, Germany.

Author Contributions

Z.D. and J.P.S. conceived of the project. Z.D. fabricated and characterized the stealth surfaces. M.K. and R.B. carried out the simulations. Z.D., J.-H.D., and J.P.S. analyzed the data and drafted the manuscript. All authors commented on the manuscript.

Notes

The authors declare no competing financial interest.

■ ACKNOWLEDGMENTS

We thank J. Hirte for the help of AFM measurements and contamination test. We thank Dr. J. Overbuschmann and Dr. R. Huber from Trumpf Laser GmbH for providing us samples in LIDT measurements and useful discussions. This study was financially supported by the BMBF VIP scheme and the Max Planck Society. J.P.S. is the Weston Visiting Professor at the Weizmann Institute of Science and part of the excellence cluster CellNetworks at the University of Heidelberg.

■ REFERENCES

(1) Clapham, P. B.; Hutley, M. C. *Nature* **1973**, *244* (5414), 281−282.
(2) Vukusic, P.; Sambles, J. R. *Nature* **2003**, *424* (6950), 852−855.
(3) Huang, Y. F.; Chattopadhyay, S.; Jen, Y. J.; Peng, C. Y.; Liu, T. A.; Hsu, Y. K.; Pan, C. L.; Lo, H. C.; Hsu, C. H.; Chang, Y. H.; Lee, C. S.; Chen, K. H.; Chen, L. C. *Nat. Nanotechnol.* **2007**, *2* (12), 770−774.
(4) Xi, J. Q.; Schubert, M. F.; Kim, J. K.; Schubert, E. F.; Chen, M. F.; Lin, S. Y.; Liu, W.; Smart, J. A. *Nat. Photonics* **2007**, *1* (3), 176−179.
(5) Rahman, A.; Ashraf, A.; Xin, H. L.; Tong, X.; Sutter, P.; Eisaman, M. D.; Black, C. T. *Nat. Commun.* **2015**, *6*, 5963.

DOI: 10.1021/acs.nanolett.6b03308
Nano Lett. XXXX, XXX, XXX−XXX

(6) Savin, H.; Repo, P.; von Gastrow, G.; Ortega, P.; Calle, E.; Garin, M.; Alcubilla, R. *Nat. Nanotechnol.* **2015**, *10* (7), 624−629.
(7) Kikuta, H.; Toyota, H.; Yu, W. J. *Opt. Rev.* **2003**, *10* (2), 63−73.
(8) Rosfjord, K. M.; Yang, J. K. W.; Dauler, E. A.; Kerman, A. J.; Anant, V.; Voronov, B. M.; Gol'tsman, G. N.; Berggren, K. K. *Opt. Express* **2006**, *14* (2), 527−534.
(9) Kim, J. K.; Chhajed, S.; Schubert, M. F.; Schubert, E. F.; Fischer, A. J.; Crawford, M. H.; Cho, J.; Kim, H.; Sone, C. *Adv. Mater.* **2008**, *20* (4), 801−804.
(10) Jannasch, A.; Demirors, A. F.; van Oostrum, P. D. J.; van Blaaderen, A.; Schaffer, E. *Nat. Photonics* **2012**, *6* (7), 469−473.
(11) Rayleigh, J. S. *Proc. London Math. Soc.* **1880**, *11*, 51−56.
(12) Yang, Z. P.; Ci, L. J.; Bur, J. A.; Lin, S. Y.; Ajayan, P. M. *Nano Lett.* **2008**, *8* (2), 446−451.
(13) Wilson, S. J.; Hutley, M. C. *Opt. Acta* **1982**, *29* (7), 993−1009.
(14) Zhang, J. H.; Yang, B. *Adv. Funct. Mater.* **2010**, *20* (20), 3411−3424.
(15) Sivakov, V.; Andra, G.; Gawlik, A.; Berger, A.; Plentz, J.; Falk, F.; Christiansen, S. H. *Nano Lett.* **2009**, *9* (4), 1549−1554.
(16) Vaissie, L.; Smolski, O. V.; Mehta, A.; Johnson, E. G. *IEEE Photonics Technol. Lett.* **2005**, *17* (4), 732−734.
(17) Yu, P. C.; Chang, C. H.; Chiu, C. H.; Yang, C. S.; Yu, J. C.; Kuo, H. C.; Hsu, S. H.; Chang, Y. C. *Adv. Mater.* **2009**, *21* (16), 1618−1621.
(18) Spatz, J. P.; Mossmer, S.; Hartmann, C.; Möller, M.; Herzog, T.; Krieger, M.; Boyen, H. G.; Ziemann, P.; Kabius, B. *Langmuir* **2000**, *16* (2), 407−415.
(19) Glass, R.; Arnold, M.; Blummel, J.; Kuller, A.; Möller, M.; Spatz, J. P. *Adv. Funct. Mater.* **2003**, *13* (7), 569−575.
(20) Wilcoxon, J. P.; Abrams, B. L. *Chem. Soc. Rev.* **2006**, *35* (11), 1162−1194.
(21) Lohmuller, T.; Helgert, M.; Sundermann, M.; Brunner, R.; Spatz, J. P. *Nano Lett.* **2008**, *8* (5), 1429−1433.
(22) Lehr, D.; Helgert, M.; Sundermann, M.; Morhard, C.; Pacholski, C.; Spatz, J. P.; Brunner, R. *Opt. Express* **2010**, *18* (23), 23878−23890.
(23) Brown, K. R.; Natan, M. J. *Langmuir* **1998**, *14* (4), 726−728.
(24) Brown, K. R.; Walter, D. G.; Natan, M. J. *Chem. Mater.* **2000**, *12* (2), 306−313.
(25) Southwell, W. H. *Opt. Lett.* **1983**, *8* (11), 584−586.
(26) Siddique, R. H.; Gomard, G.; Holscher, H. *Nat. Commun.* **2015**, *6*, 6909.
(27) Gombert, A.; Glaubitt, W.; Rose, K.; Dreibholz, J.; Blasi, B.; Heinzel, A.; Sporn, D.; Doll, W.; Wittwer, V. *Sol. Energy* **2000**, *68* (4), 357−360.
(28) Ibn-Elhaj, M.; Schadt, M. *Nature* **2001**, *410* (6830), 796−799.
(29) Mcclung, F. J.; Hellwarth, R. W. *J. Appl. Phys.* **1962**, *33* (3), 828−829.
(30) Ristau, D.; Jupe, M.; Starke, K. *Thin Solid Films* **2009**, *518* (5), 1607−1613.
(31) Fan, F.; Turkdogan, S.; Liu, Z. C.; Shelhammer, D.; Ning, C. Z. *Nat. Nanotechnol.* **2015**, *10* (9), 796−803.
(32) Hobbs, D. S.; MacLeod, B. D.; Sabatino, E., III; Hartnett, T. M.; Gentilman, R. L. *Proc. SPIE* **2011**, 8016.

DOI: 10.1021/acs.nanolett.6b03308
Nano Lett. XXXX, XXX, XXX−XXX